Theor Chem Acc (2007) 117:933–942
DOI 10.1007/s00214-006-0214-1

REGULAR ARTICLE

A computational multiscale strategy to the study of amorphous materials

G. Malavasi · M. C. Menziani · A. Pedone · B. Civalleri · M. Corno · P. Ugliengo

Received: 21 June 2006 / Accepted: 13 October 2006 / Published online: 28 February 2007

Abstract A first step towards a computational multiscale approach has been adopted here to deal with the computational simulation of the Hench bioglass® 45S5, an amorphous material of 48.1% SiO_2, 25.9% CaO, 22.2% Na_2O and 3.7% P_2O_5 composition. Molecular dynamics simulations based on classical force fields followed by static minimizations on quenched structures have been run on a unit cell size suitable for subsequent ab initio calculations. The molecular mechanics optimized unit cell envisaging 78 atoms of $Na_{12}Ca_7P_2Si_{13}O_{44}$ composition and P1 symmetry has then been fully optimized (both unit cell parameters and internal coordinates) at B3LYP level in a periodic approach using gaussian basis sets of double-ζ quality and the development version of the CRYSTAL03 code. Comparison between the molecular mechanics and B3LYP optimized structures shows the latter to give a slightly higher density than the former, due to overestimation of the Si–O bonds and underestimation of the Si–O–Si and Si–O–P angles, respectively. Other geometrical features are in excellent agreement within the two approaches. Electronic properties of the Hench bioglass have been reported at B3LYP for the first time and both Mulliken charges and electronic band structure show a rather ionic character of the material, whereas a band gap of about 6.5 eV characterizes the bioglass as a strong insulator. Work presently in progress will soon allow the information to be transferred from the B3LYP calculations to the molecular mechanics engine in order to refine the presently available empirical force fields for complex ionic systems and their surfaces.

Electronic supplementary material The online version of this article (doi:10.1007/s00214-006-0214-1) contains supplementary material, which is available to authorized users.

G. Malavasi · M. C. Menziani (✉) · A. Pedone
Department of Chemistry and SCS center,
University of Modena and Reggio Emilia,
Via G.Campi 183, 41100 Modena, Italy
e-mail: menziani@unimo.it

B. Civalleri · M. Corno · P. Ugliengo (✉)
Dipartimento di Chimica IFM, NIS Centre of Excellence
and INSTM (Materials Science and Technology)
National Consortium, UdR Torino,
Via P. Giuria 7, Torino, Italy
e-mail: piero.ugliengo@unito.it

1 Introduction

The computational modelling of amorphous solids is a difficult task, the immediate difficulty arising from the need to obtain atomistic models (coordinates of the atoms) that reproduce the known experimental features of the material. This is because no currently conceivable set of experiments leads to a unique structure of an amorphous compound and there is no rigorous definition of when it has been determined.

Molecular dynamics (MD) simulations may be considered the intuitive natural way to make a computer model of an amorphous or glassy material. In this framework, an equilibrated liquid is cooled through the glass transition to the final solid structure. Periodically repeated units are usually utilized, and the faulty assumption of periodicity is compensated by the use of large unit cells. Recent ab initio molecular dynamics simulations have provided very accurate data on the local structure and electronic properties of amorphous silica or simple silicate glasses [1–3]. Unfortunately, at

present, the size and time scales which can be probed by ab initio molecular dynamics are limited to few hundreds of atoms and tens of picoseconds.

Classical molecular dynamics (MD) simulations allow the study of structural, mechanical, thermodynamical and dynamical properties of relatively large systems (of the order of 10^4–10^5 atoms) for long time scales (order of ns). However, the reliability of the results obtained strongly depends on the adequacy of the description of the inter-atomic potential, acting on the constituent ions.

The aspect most frequently questioned regards the limited validity of the force-field utilized. It is generally assumed that empirical parameters are best used within the class they have been fitted. Parameters for amorphous materials are typically obtained from fitting to a set of experimental data measured on crystalline solids and therefore their domain of applicability has to be clearly understood and identified.

Moreover, a fundamental difference to harmonic force fields used for organic molecules and biopolymers consists in the difficulty of establishing a clear separation between bonding and non-bonding interactions in the amorphous material. Bonding in alkaline and alkaline-earth silicate glasses exhibits partially ionic and partially covalent character and further complications for parameterisation arise for multicomponent glasses containing asymmetric network forming cations, such as B^{3+} or P^{5+}. In addition, bond breaking and forming events can occur at the high temperatures used for glass synthesis; thus the coordination number might vary for a pair of elements during simulations. Finally, in amorphous materials, irregularities may occur and, in general, under- and over-coordinations should not be ruled out.

Recent advances in the interatomic potential energy functions allow the correct quantitative estimation of the numerical value of structural, mechanical, thermo-physical, and transport properties for simple glasses [4–7].

Moreover, deep understanding of composition–atomic structure relationships and insight into the reactivity of multicomponent glasses have been achieved [8–11]. However, accurate and reliable descriptions of second-order properties for multicomponent glasses have proved far more difficult, although general trends that are consistent with experimental results can be obtained [12]. With the inclusion of polarization effects into empirical potential and the development of ab initio derived parameters, theoretical analysis of properties besides structure has become appropriate [13,14].

To help in the development and assessment of new interatomic potentials for classical force field of multicomponent glasses with special attention, in the long term, to the description of glass surfaces and processes occurring there, we attempt in this paper the computational simulation of the Hench Bioglass® (45S5 glass composition: 48.1% SiO_2, 25.9% CaO, 22.2% Na_2O and 3.7% P_2O_5 % mol) by means of an ab initio local basis set based periodic treatment as coded in CRYSTAL03 program [15]. It is worth noting that the studied glass is of great interest in medical applications since in the presence of body fluids, and depending upon the rate of ion release and resorption, it creates chemical gradients which promote the formation of a layer of biologically active bone-like hydroxyapatite at the implantation interface. Osteoblasts can preferentially proliferate on the apatite layer, and differentiate to form new bone that bonds strongly to the implant surface.

The long range target of modelling such complex processes occurring at the bioglass surface in a computational fashion is very ambitious and challenging. Here, the first step of a multiscale strategy is proposed in order to meet this goal; this involves the combined use of MD based on classical molecular mechanics (MM) force fields to generate the glass structure as a starting point for a full ab initio static geometry optimization based on the best DFT hamiltonians, i.e. hybrid functionals as B3LYP, to fully characterize the structural and electronic properties of the glass.

2 Computational procedure

2.1 Generation of the amorphous structure by classical MD simulations

In the cases of amorphous solids, as glasses, X-ray or neutron diffraction experiments only provide one dimensional information (correlation functions), therefore, a full three dimensional reconstruction of the atomic structure is not possible, and recourse to modelling is somewhat essential. The glass samples were generated by means of classical MD simulations with a recently published self-consistent force field explicitly derived for oxides, silicate and glasses [12]. A box containing 78 atoms with cell size of 10.10 Å per side, calculated accordingly with the experimental density of 2.72 g/cm^3, was considered. The initial position of each atom was randomly generated. The leap-frog Verlet integrator and a timestep of 2 fs were used to perform MD simulations with the GULP package [16]. The system was then heated at 6,000 K, a temperature more than adequate to bring the system to its liquid state in the framework of the adopted force field, which assigns partial charges to atoms. The melt was then equilibrated for 100 ps and subsequently cooled down continuously from 6,000 to 300 K in 1,140 ps with a nominal cooling

rate of 5 K/ps. The temperature was decreased by 0.01 K every timestep using Nose–Hoover thermostat [17] with the time constant parameter for the frictional coefficient set to 0.1 ps. The cooling protocol influences the results of the simulations and the one adopted here has been optimized by comparing the simulated total neutron distribution function, broadened as described by Wright [18], with those obtained experimentally for silica and sodium silicate glasses.

Simulations were carried out in the constant volume NVT ensemble. Another 100 ps of equilibration at constant energy and 50 ps of data production were performed at 300 K. Configurations at every 0.1 ps were recorded for structural analysis.

Finally, static energy minimizations at constant P and constant V were carried out on the obtained MD configurations. The one chosen as a starting point for the periodic ab initio full geometry relaxation is considered to be representative of the different structural features observed for the constituting atoms during the glass forming dynamic procedure.

2.2 Technical considerations

Glasses are considered to possess an infinite unit cell because of the lacking of long range order, so that in this framework, big simulation cells with periodic boundary conditions and minimum image convention are usually used to evaluate the pair interaction between ions. Defining unit cell size adequate for ab initio treatment from these large systems is not trivial, since both electroneutrality and the correct density of the system have to be maintained. One possible solution is then to generate the amorphous structure using a unit cell small enough to be handled at ab initio level. A reasonable compromise, has however, to be reached in order to avoid a too small unit cell size which will suffer of poor statistical averaging. Moreover, technical problems arise for the choice of the cut-offs employed in the evaluation of Coulombic and van der Waals interactions.

The pair-potentials used in this paper were recently derived [12] by fitting structural and mechanical aspects of oxides and several silicate crystals using a short range cut-off of 15.0 Å ; the Coulombic interactions were evaluated by the Ewald summation with no minimum image convention, within the GULP package [16]. In the simulation of glasses, the short range cut-off should be optimized with respect to the dimension of the box. Besides taking into account the computational effort, long cut-offs lead to negative pressures in constant volume simulations and glass densities higher than the experimental one in constant pressure simulations. On the other hand, short cut-offs give rise to instabilities in the integrations affecting convergence.

Several tests carried out in our lab showed that an appropriate short range cut-off for the adopted potential is 5.5 Å . This is longer than half the simulation cell edge length; therefore, the minimum image convention was not applied here.

As already stated, the electrostatic interactions usually are evaluated through the Ewald summation method [19]. In this method, the Coulombic term is subjected to a Laplace transformation and then separated into two components, one of which is rapidly convergent in real space, and a second which decays quickly in reciprocal space. The resulting expressions for real and reciprocal space are:

$$U^{\text{real}} = \frac{1}{2}\sum_{i=1}^{N}\sum_{j=1}^{N}\frac{q_i q_j}{r_{ij}}\text{erfc}\left(\eta^{1/2} r_{ij}\right) \tag{1}$$

$$U^{\text{recip}} = \frac{1}{2}\sum_{i=1}^{N}\sum_{j=1}^{N}\sum_{G}\frac{4\pi}{V} q_i q_j \text{e}^{(iG\cdot r_{ij})}\frac{\text{e}^{-\frac{G^2}{4\eta}}}{G^2} \tag{2}$$

where q is the charge on an ion, G is a reciprocal lattice vector (where the special case $G = 0$ is excluded), V is the volume of the unit cell, and η is a parameter that controls the division of work between real and reciprocal space. The above equations still require the choice of cut-offs for real and reciprocal space. One approach to determine these in a consistent fashion is to minimise the total number of terms to be evaluated in both the series for a given specified accuracy [20]. This leads to the following expressions:

$$\eta_{\text{opt}} = \left(\frac{N\omega\pi^3}{V}\right)^{1/3} \tag{3}$$

$$r_{\text{max}} = \left(\frac{-\ln(A)}{\eta}\right)^{1/2} \tag{4}$$

$$G_{\text{max}} = 2\eta^{1/2}(-\ln(A))^{1/2} \tag{5}$$

The above expressions contain one difference from the original derivation, in that a weight parameter, ω, has been included in the GULP code that represents the relative computational expense of calculating a term in the real and reciprocal space, respectively. Tuning of this parameter can lead to significant benefits for large systems. In the present work the accuracy has been set to 10^{-8} and ω to 1.0 that are the default values within the GULP code.

2.3 Geometry optimization with CRYSTAL03

The structure of the bioglass obtained by the MM procedure previously described, has then been optimized with

the ab initio CRYSTAL03 program [15] with two different Hamiltonians, namely Hartree–Fock and the hybrid functional B3LYP. The starting structure of $Na_{12}Ca_7P_2Si_{13}O_{44}$ composition contains 78 atoms in a cubic cell ($a = b = c = 10.10$ Å, $\alpha = \beta = \gamma = 90°$) (see Table 1, third column). The basis set adopted is an all-electron extended Gaussian-type function (GTF) basis set. For Ca ions, the first ten electrons (shell 1 and 2) are represented by the effective core pseudopotential of Hay and Wadt [21,22], while three contracted GTF are used for the remaining ten electrons (shell orbital 3sp and 4s) and one GTF for the outer sp shell (basis [HAY-WSC]-31G) [23]. The exponents of the most diffuse shells are $\alpha_{sp} = 0.5\,\text{bohr}^{-2}$. Na ions are described by a 8-511G basis set [24–28] (most diffuse shell exponents $\alpha_{sp} = 0.323\,\text{bohr}^{-2}$). Si atoms adopt a 6-21G(d) modified basis set (most diffuse shell exponent $\alpha_{sp} = 0.13$ and $\alpha_d = 0.5\,\text{bohr}^{-2}$ for polarization functions), whereas P atoms is described by a 85-21G(d) basis set with most diffuse shell exponent $\alpha_{sp} = 0.135\,\text{bohr}^{-2}$ and $\alpha_d = 0.74583\,\text{bohr}^{-2}$ for polarization, respectively. Oxygen atoms are described with a 6-31G(d) basis set with the most diffuse shell exponents $\alpha_{sp} = 0.2742\,\text{bohr}^{-2}$ and $\alpha_d = 0.538\,\text{bohr}^{-2}$ for polarization. The total number of atomic orbitals amounts to 1,098 functions.

Table 1 Structural properties (average values) determined after MM at constant V, MM at constant P and DFT optimization with the B3LYP functional

	MM (V = cost)	MM (P = cost)	B3LYP
a (Å)	10.10	9.92	9.42
b (Å)	10.10	9.89	10.24
c (Å)	10.10	10.51	10.34
α(°)	90.0	88.9	88.7
β(°)	90.0	92.1	91.7
γ(°)	90.0	87.7	86.0
V_{cell}(Å^3)	1030.3	1029.2	993.9
d(g/cm^3)	2.72	2.72	2.82
Si-O	1.607	1.606	1.658
c.n.	4.0	4.0	3.7
Si–NBO	1.573	1.569	1.604
Si–BO	1.620	1.634	1.666
P–O	1.522	1.522	1.554
c.n.	4.0	4.0	4.0
P–NBO	1.518	1.518	1.542
P–BO	1.552	1.552	1.648
Ca–O	2.479	2.472	2.436
c.n.	6.0	6.0	6.3
Ca–NBO	2.453	2.436	2.443
Ca–BO	2.737	2.761	2.611
Na–O	2.465	2.490	2.365
c.n.	5.3	5.7	5.0
Na–NBO	2.420	2.434	2.390
Na–BO	2.621	2.680	2.722
O–O	2.598	2.598	2.692
Si–Si	3.102	3.100	3.064
Ω (O–Si–O)	109.2	109.4	109.4
Ω (O–P–O)	109.4	109.4	109.5
Ω (Si–O–Si)	146.5	144.4	135.6
Ω (P–O–Si)	171.0	169.0	138.0

(All the calculations have been performed starting from the same initial structural model. Bond lengths are in Å, bond angles in degrees)

The ab initio simulation has been divided in two different macro steps. First, the unit cell parameters were fixed at a given value while the fractional coordinates were fully relaxed. In a subsequent step, the unit cell parameters were relaxed and the procedure repeated until convergence was achieved. This procedure was carried out manually, since the CRYSTAL03 public version could not allow for the simultaneous optimization of both set of variables. To speed up the calculation, Hartree–Fock Hamiltonian has been used as a first method, starting from the MM optimized structure. About 500 macro optimisation cycles were needed to achieve convergence, by running CRYSTAL03 on 16 IBM SP5 CPUs hosted by the CINECA Supercomputing Center (IBM SP Cluster 1600, with IBM Power5 processors running at 1.9 GHz under the AIX 5.2 operating system). To speed up convergence, initial values of the tolerances on gradient and maximum allowed geometrical displacement were set to 0.003 hartree bohr^{-1} and 0.012 bohr, respectively. These values have been then set to 0.0003 hartree bohr^{-1} and 0.006 bohr for the last part of the optimization (default values are 0.0003 hartree bohr^{-1} and 0.0012 bohr).

Starting from the HF optimized structure, Becke three-parameter (B3) hybrid exchange functional in combination with the gradient-corrected correlation functional (LYP) of Lee et al. [29,30] was used. The B3LYP functional has recently been proved to be very accurate for the treatment of ionic and covalent crystals [31,32] and has been used by some of us to study complex silicates, both as far as structures and phonons frequencies are concerned [33–35]. By using a CRYSTAL03 development version, internal coordinates and cell parameters have been optimized in a fully automatic and efficient way on 16 CPUs (SGI Altix 350 with Itanium2 Processor 3.0 MB L3 cache running at 1.3 GHz under Suse-10 Linux operating system), adopting default values of the optimization tolerances. The new implemented optimization feature of the code has allowed the optimization of the bioglass structure in less than 2 weeks of wall clock time, which is very reasonable for a system of this size in which internal coordinates and cell parameters are fully coupled. This result has also been possible due to significant improvements in the generation and handling of the integration grid in the DFT calculation, which has been fully parallelized in the CRYSTAL03 development version of the code.

Indeed, for the B3LYP calculations, the adopted grid of points over which the integration of electronic density and its gradient is performed was a pruned grid of 75 radial points and 434 angular points, divided into 5 subintervals of 50, 146, 194, 434, and 194 points (known as LGRID) resulting in about 900,000 total grid points. With this grid, the integration of the electronic density gives the total number of electron with an error of 10^{-3} electrons upon 766 total in the unit cell. For all calculations, default values of Coulomb and exchange tolerances series have been used (ITOL1 = ITOL2 = ITOL3 = ITOL4 = 6, ITOL5 = 12); Hamiltonian matrix has been diagonalized on eight reciprocal lattice points (k-points, shrinking factor IS = 2) [36] by distributing the calculation on eight different CPUs so to achieve almost linear scaling in this step as a function of k points.

3 Results and discussion

The small system size used in this study prevents the study of medium range order properties such as clustering of ions [9] and Q_n [8], ring size [37], and void size distributions [38]. Moreover, it is worth considering that also the Si–O–Si inter-tetrahedral angle distribution might be affected by the size of the simulation cell [14]. However, as shown by the presence of an energy gap in the electronic density of states of amorphous oxides and in the similarity of the vibrational spectra between amorphous and crystalline materials, short range properties govern the electronic and vibrational properties of the amorphous phases.

Therefore, the optimised structures have been analysed in terms of their structural features, focusing on the differences between the results of the classical and the quantum mechanical approaches. Investigations were carried out both by comparing computed density, lattice parameters, bond distances, and angles—values are listed in Table 1—and by graphical visualization of the distribution of each atom inside the unit cell (see Scheme 1, 2 and 3), using the molecular graphics program MOLDRAW [39].

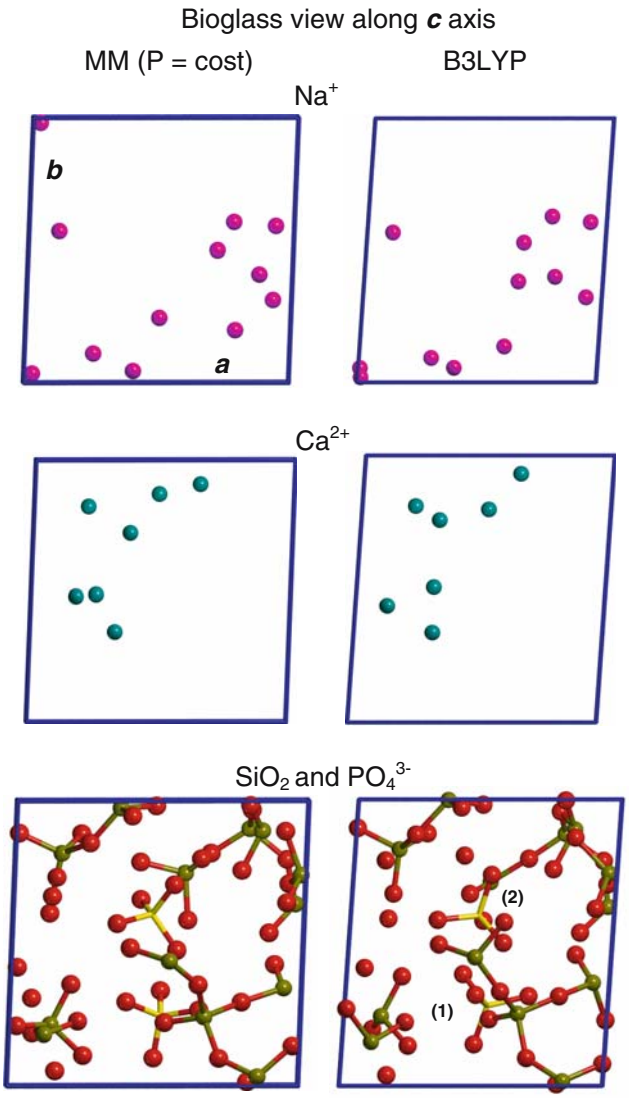

Scheme 1 Graphical representation of the Na^+, Ca^{2+}, SiO_2, and PO_4^{3-} ion distribution inside the unit cell of the Hench 45S5 bioglass, as viewed along the c axis

3.1 Structural features

3.1.1 Density

On one hand, the experimental value of 2.72 g/cm^3 imposed on constant volume MM minimization is confirmed by the calculation carried out at constant P. On the other hand, relaxation of the cell volume using the B3LYP functional leads to a density of 2.82 g/cm^3, some 3.5% higher than the experimental one.

Constant volume MM calculations adopt a cubic simulation boxe ($a = b = c = 10.10$ Å and $\alpha = \beta = \gamma = 90°$), whereas for both the constant pressure MM and B3LYP cases the optimised cell is triclinic with relatively small deviations from the cubic box. Comparison between constant P MM and B3LYP shows that the optimised unit cell of the latter (see Fig. 1) has the a and c cell parameters smaller, respectively, than ≈0.5 and 0.2 Å than the former. As for the lattice angles, the B3LYP α, β and γ values deviate from the P constant MM ones by less than 0.2°.

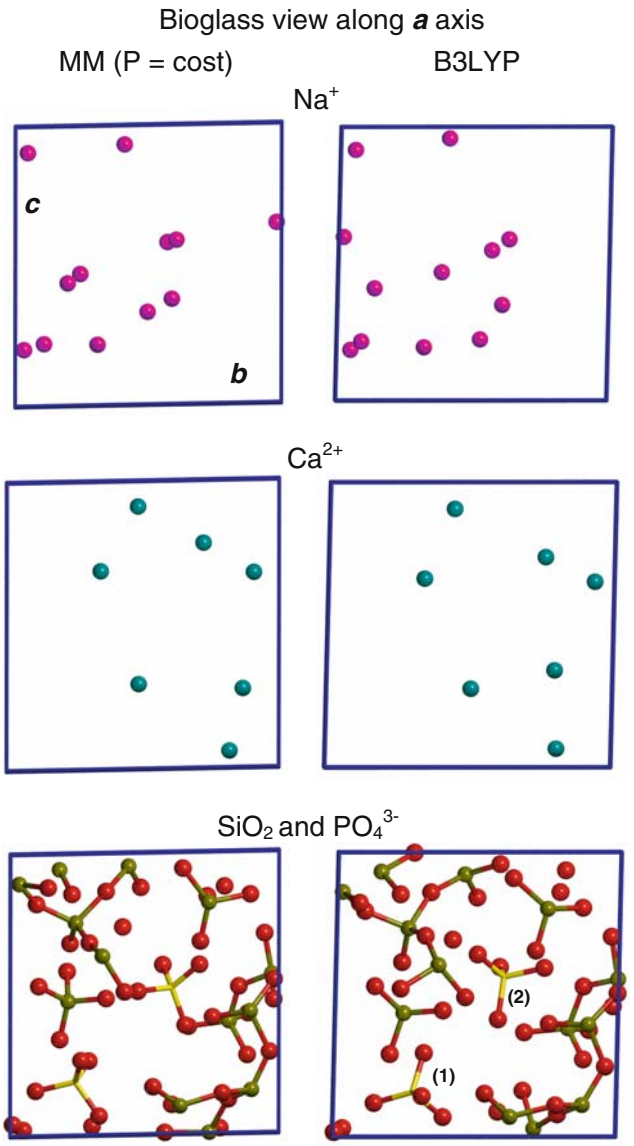

Scheme 2 Graphical representation of the Na^+, Ca^{2+}, SiO_2, and PO_4^{3-} ion distribution inside the unit cell of the Hench 45S5 bioglass, as viewed along the *a* axis

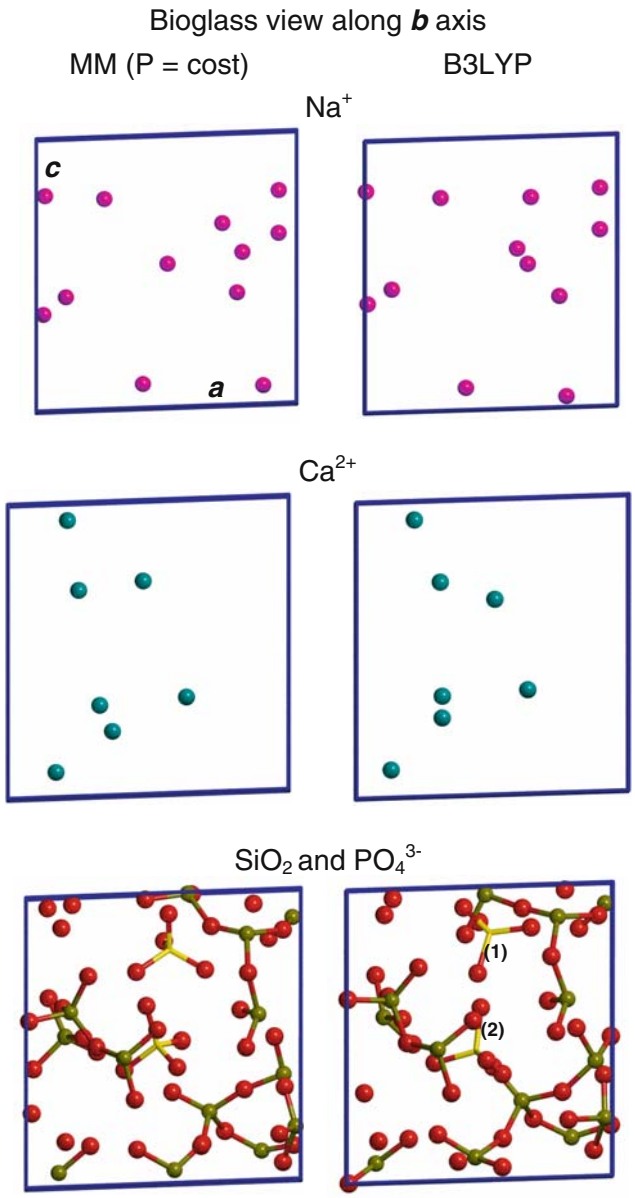

Scheme 3 Graphical representation of the Na^+, Ca^{2+}, SiO_2, and PO_4^{3-} ion distribution inside the unit cell of the Hench 45S5 bioglass, as viewed along the *b* axis

3.1.2 Bulk properties

The fundamental structure of the bioglass consists of a random network of distorted SiO_4 tetrahedra surrounded by sodium and calcium ions and of two phosphate groups, one isolated and the other linked to a SiO_4 group—in Fig. 1 and Scheme 1, 2 and 3, labelled (1) and (2), respectively. This last feature is known to be an artefact since ^{31}P MAS NMR findings [8] show that low concentrations of *P* in the Hench Bioglass® allow the random dissemination of isolated monophosphate units in the silicon network. During the MD experiments on large boxes [8,9], we observed that the occurrence of linked Si–O–P units is strongly dependent, within the framework of a chosen force field, on the annealing procedure used to obtain the glass structure. However, small percentages of linked Si and P tetrahedra were always found and this occurrence can be considered a defect when large numbers of atoms are considered. To reproduce the statistical distribution observed in large boxes, multiple small unit cells should be considered for ab initio calculations. While working is in progress to address this issue, in this preliminary paper, a configuration representative of both the possible structural features of the *P* atom has been chosen as a starting point for the

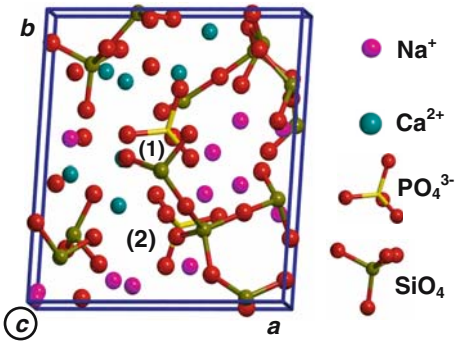

Fig. 1 View along the *c* axis of the B3LYP Hench 45S5 bioglass optimised unit cell. The unit cell contains 78 atoms with $Na_{12}Ca_7P_2Si_{13}O_{44}$ composition

periodic ab initio full geometry relaxation with the aim of verifying the local stability of the *P* environment.

The detailed analysis of the geometrical features of the tetrahedral network and the coordination environment of the modifier ions allows a clearer description of the computed structures. Relevant geometrical features of the optimised structures are also listed in Table 1.

The average Si–O bond length obtained by the B3LYP functional of 1.658 Å is longer than the average values obtained by means of MM constant volume (1.607 Å) and constant pressure (1.606 Å) calculations.

It is generally assumed [40] that the local structure of a glass is similar to that of the phases separated by glass crystallisation, therefore, the structural features of the crystal phases obtained after thermal treatment [9] might constitute a validation of the computational results.

For the Hench Bioglass, the $Na_2CaSi_2O_6$ crystal phase is the ternary sodium–calcium silicate identified as main phase in the XRD pattern after 2.5 h of thermal treatment. In this crystal phase, the average Si–O bond length is 1.601 Å. This is given by the two contributions of Si–BO (1.619 Å) and Si–NBO (1.575 Å), where BO is a bridging oxygen and NBO is a non-bridging oxygen. Classical parameters provide an average Si–BO bond length that ranges from 1.620 to 1.634 Å, and an average Si–NBO bond length that ranges from 1.569 to 1.573 Å, depending on the adopted ensamble. These values are longer at B3LYP level being 1.666 and 1.604 Å for Si–BO and Si–NBO, respectively. This fact is a well known weakness of B3LYP and other pure GGA functionals in predicting Si–O bond lengths which result too long [41]. An under-coordinated Si defect is also found in the quantum–mechanical calculation leading to an average coordination number of 3.7 oxygen atoms around Silicon. Similarly, the B3LYP Si–Si and O–O distances are longer than those observed in the MM minimized structures, for which the average values are respectively 3.1 and 2.60 Å .

Concerning the phosphates groups, there are two different cases inside the unit cell, as already mentioned: (1) and (2), the first of which is isolated while the second group is linked to a SiO_4 tetrahedron. The classical approaches provide an average P–NBO bond length around 1.52 Å, while the B3LYP functional provides an average P–O about 1.554 Å that is mainly made up by the P–NBO contribution at 1.542 Å. Recent experimental studies carried out by some of us [8,9] showed that when the molar percentage of P_2O_5 in the parent bioglass is augmented to 5% mol and more, the β-$NaCaPO_4$ crystal phase crystallizes after thermal treatment. This is an othophosphate, in which the P–O bond lengths range from 1.477 to 1.604 Å with an average distance at 1.536 Å.

The O–Si–O and O–P–O bond angles are all very well reproduced and compare well with the experimental angles found in the $Na_2CaSi_2O_6$ and β-$NaCaPO_4$ which are 109.3 and 109.4° respectively. Pictures displayed in Schemes 1, 2 and 3 reveal that phosphate groups are differently spatially oriented in the unit cell of the B3LYP structure when compared to the constant pressure MM one. This fact is probably a consequence of the different P–BO distances and it can be due to the differences in the silica framework previously outlined and to the definitely smaller B3LYP P–O–Si angle (average value ≈138°) in comparison to the value of ≈ 170° for the MM cases.

The Si–O–Si and P–O–Si angles show B3LYP average values which are always too small than the corresponding MM ones. In general, changes of these angles correspond to relatively modest variations in energy, so that the final values are sensitive to both adopted functional and basis set. Because these geometrical parameters control the bioglass density, their underestimation at B3LYP level is the main reason (together with the Si–O overestimation) of a lower computed density with respect to the experimental one. Visual inspection of the last rows of Schemes 1, 2 and 3 shows a slightly more compact silicon framework at B3LYP when compared to the MM case.

The local environment of calcium ions inside the bioglass is very similar in the MM and B3LYP methods. The average Ca–O bond lengths of 2.47–2.48 Å at MM level and 2.44 Å at B3LYP compare well with the average Ca–O bond length of 2.459 Å in the ternary silicate crystal and of 2.477 Å for the β-$NaCaPO_4$ crystal. Small differences are observed in the environment around modifier cations, as Ca ion is surrounded, as an average, by 6.0 oxygen atoms when MM is adopted and by 6.3 at the B3LYP level. Indeed, inspection of

Schemes 1, 2 and 3 reveals very few differences in the distributions of Ca ions between the two computational methods.

Finally, the average Na–O distances ranges between 2.46 to 2.49 Å, with coordination numbers between 5.3 and 5.7 at MM level to be compared with a distance of 2.365 Å and a coordination number of 5 oxygen atoms for the B3LYP case. These distances range between 2.35 and 2.72 Å in the $Na_2CaSi_2O_6$ crystal, with coordination number between 6 and 8, whereas in the orthophosphate crystal the average Na–O distance is 2.644 Å and 8 oxygen atoms around Na are found.

3.2 Electronic properties

The ab initio B3LYP calculation provides, besides geometrical structures, electronic features of the 45S5 bioglass, as Mulliken atomic net charges, the band structure and density of states. As for the Mulliken net charges, it results that the average values are 0.872, 2.054, −2.887 and −2.333 electrons for Na, Ca, $PO_4(1)$ and $PO_4(2)$, respectively. Although it is known that Mulliken charges are relatively dependent on the adopted basis set, the present values clearly indicate that the Hench bioglass is an ionic material; indeed, Na and Ca net charges are very close to the formal ionic charges of +1 and +2, respectively. Interestingly, whereas Na acquires about 0.128 electrons from the surrounding, thus, decreasing its formal +1 net charge, Ca looses about 0.054 electrons. As for the PO_4 groups, Mulliken net charges confirm the different nature of $PO_4(1)$ and $PO_4(2)$ groups, since $PO_4(1)$ bears a charge closer to the formal ionic charge of −3 than $PO_4(2)$, in agreement with the isolated nature of the $PO_4(1)$ group in comparison with $PO_4(2)$, which is linked to a Si atom of the silica framework.

Band structure is calculated in the Brillouin zone along the path Γ–B–F–G–Γ with coordinates of the four k points as: $\Gamma = (0\ 0\ 0)$; $B = (1/2\ 0\ 0)$; $F = (0\ 1/2\ 0)$ and $G = (0\ 0\ 1/2)$. Figure 2a displays the resulting band structure diagram along this path, showing a rather featureless and flat structure compatible with the ionic nature of the bioglass, whereas the band gap of about 6.5 eV shows its insulating nature. The total and projected density of states (DOS) are plotted in Fig. 2b and show a direct correspondence with the band structure, allowing the identification of the specific contribution of the orbitals of each chemical species in the unit cell. Thus, whereas Ca ions DOS fall in the lower end of the energy range, Na ions states are closer to the Fermi level. Silicon and oxygen DOS are the broadest, with levels extending close to the Fermi level. Also phosphorous DOS, beside a peak deep in energy, contributes to the DOS close to the Fermi level.

4 Conclusions

In this work, the first step in a multiscale approach for the computational simulation of a material as

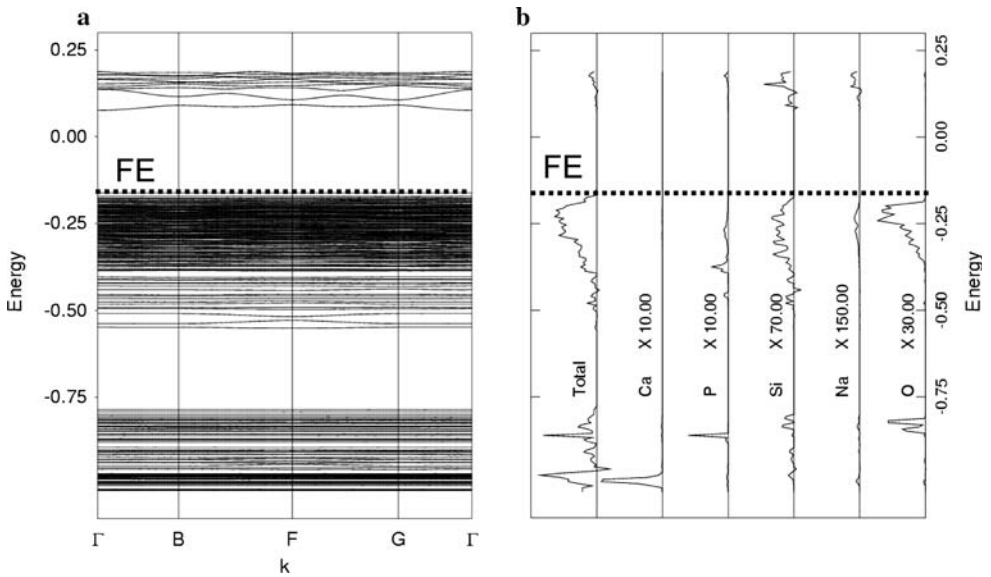

Fig. 2 B3LYP band structure (**a**) and corresponding density of states (**b**) (total and projected on each atomic species) of the Hench 45S5 bioglass structure; Fermi energy (FE) level indicated by the *dotted line*. Please note that different multiplicative factors are used to enlarge the atomic DOS

complex as the Hench bioglass® of 45S5 of 48.1% SiO_2, 25.9% CaO, 22.2% Na_2O and 3.7% P_2O_5 composition has been undertaken. To achieve such a goal, molecular dynamics simulations based on classical force fields have been carried out on a unit cell containing 78 atoms with $Na_{12}Ca_7P_2Si_{13}O_{44}$ composition and P1 symmetry. Molecular mechanics minimization was then run on a representative quenched structure, to relax fully the system which is subsequently passed to the CRYSTAL code as a starting structure to perform a full ab initio periodic geometry relaxation using the hybrid B3LYP functional with gaussian basis sets of double-ζ quality. The hybrid B3LYP has been chosen because it has recently proved to be very successful in the treatment of complex silicate crystals [32–35]. Notwithstanding, more definitive conclusions could be drawn only by averaging information on multiple small unit cells in the attempt of reproducing the statistical distribution of structures observed in large boxes, some important points can be highlighted.

B3LYP optimized structures show a slightly higher density than the one computed with the molecular mechanics approach, the latter being also in good agreement with the experimental one. This is due to a known weakness of many GGA and hybrid functionals which overestimate the Si–O bonds and underestimate the Si–O–Si and Si–O–P angles, respectively. Ca and Na distributions are in very good agreement with the two approaches, as it is the local environment around the two PO_4 groups. The B3LYP calculations also provide electronic features of the Hench bioglass, obviously unavailable from the molecular mechanics calculation. Mulliken net charges are close to the formal ionic charges showing the ionic nature of the bioglass, whereas the large band gap of 6.5 eV shows, as expected, its strong insulating character.

The present attempt is the starting point of a more general multiscale approach, in which molecular mechanics calculations will provide initial structures for ab initio simulation. The latter, in turn, will provide electronic features of complex materials and can also be used to refine, in a fully ab initio fashion, the force field parameters derived empirically. Present DFT functionals (hybrid ones in particular) have been proved as excellent tools for the simulation of static and dynamic properties of silica-based materials. On the one hand, systematic overestimation of the calculated Si–O bond lengths with the present functionals, may hamper the derivation of a fully ab initio force field competitive in accuracy with those derived empirically from experimental data; on the other hand, many materials are simply too complex to be modeled with the empirically force field derived on simpler systems, so that first principles calculations will provide a unique way to define new force fields apt to deal with the complexity of biomaterials like the Hench bioglass. This is particularly true when the surfaces of such materials are the target of interest, for which, basically no experimental data are available for the derivation of suitable force fileds. Work is actually in progress in our laboratories on model systems like hydroxyapatite, in order to derive a force field from B3LYP static and dynamic computed data (infrared spectrum) for the accurate simulation of this material which is so important for the bioglass functionality [42].

Acknowledgments The staff of the Theoretical Chemistry Research Group of the Torino University is kindly acknowledged for providing the development versions of the CRYSTAL code. Financial support from the Italian Ministry MIUR (Project COFIN2003, Prot. 2003032158 coordinated by Professor C. Morterra "The interface between silica-based materials and biomolecules and/or cell models") and computer allowance from the CINECA supercomputing center are acknowledged.

Electronic supplementry material

1. Hench bioglass 45S5 MM (constant *P*) unit cell, fractional XYZ coordinates
2. Hench bioglass 45S5 MM (constant *V*) unit cell, fractional XYZ coordinates
3. Hench bioglass 45S5 B3LYP unit cell, fractional XYZ coordinates
4. GULP input of the MM (constant *V*) Hench bioglass 45S5, in case of the constant *P* calculation, substitute the keyword conv with the keyword conp
5. CRYSTAL input of the Hench bioglass 45S5

References

1. Ispas S, Benoit M, Jund P, Jullien R (2001) Phys Rev B 64:214206
2. Tilocca A, de Leeuw NH (2006) J Mater Chem 16:1950
3. Van Ginhoven RM, Jonsson H, Corrales LR (2005) Phys Rev B 71:024208
4. Smith W, Greaves GN, Gillan MJ (1995) J Chem Phys 103:3091
5. Oviedo J, Fernandez S (1998) Phys Rev B 58:9047
6. Cormack AN, Cao Y (1996) Mol Eng 6:183:227
7. Garofalini SH (2001) In: Cygan RT, Kubicki JD (eds) Reviews in mineralogy geochemistry, vol 42, Chapter 5. Geochemical Society, Mineralogical Society of America, Washington DC, pp 131–164
8. Linati LL, G., Malavasi G, Menabue L, Menziani MC, Mustarelli LP, Segre U (2005) J Phys Chem B 109:4989
9. Lusvardi G, Malavasi G, Menabue L, Menziani MC, Pedone A, Segre U (2005) J Phys Chem B 109:21586
10. Lusvardi G, Menabue L, Menziani MC (2002) J Phys Chem B 106:9753

11. Lusvardi G, Menabue L, Menziani MC, Segre U, Ubaldini A (2004) J Non-Cryst Solids 710:345–346
12. Pedone A, Malavasi G, Menziani MC, Cormack AN, Segre U (2006) J Phys Chem B 110:11780
13. Wilson M, Walsh TR (2000) J Chem Phys 113:9180
14. Tilocca A, de Leeuw NH, Cormack AN (2006) Phys Rev B 73:104209
15. Saunders VR, Dovesi R, Roetti C, Orlando R, Zicovich-Wilson CM, Harrison NM, Doll K, Civalleri B, Bush IJ, D'Arco P, Llunell M (2003) CRYSTAL2003 User's Manual. University of Torino, Torino
16. Gale JD, Rohl AL (2003) Mol Simul 29:291
17. Hoover WG (1985) Phys Rev A 31:1695
18. Wright AC (1993) In: Simmons CJ, El-Bayoumi OH (eds) Experimental techniques of glass science. American Ceramic Society, Westerville, pp 205
19. Ewald PP (1921) Ann Phys 64:253–287
20. Gale JD (1996) Phil Mag B 73:3
21. Hay PJ, Wadt WR (1985) J Chem Phys 82:299
22. Hay PJ, Wadt WR (1985) J Chem Phys 82:284
23. Habas MP, Dovesi R, Lichanot A (1998) J Phys Cond Matter 10:6897
24. Prencipe M, Pascale F, Zicovich-Wilson CM, Saunders VR, Orlando R, Dovesi R (2004) Phys Chem Miner 31:1–6
25. Aprà E, Causà M, Prencipe M, Dovesi R, Saunders VR (1993) J Phys Condens Matter 5:2969
26. Dovesi R, Roetti C, FreyriaFava C, Prencipe M, Saunders VR (1991) Chem Phys 156:11
27. Lichanot A, Aprà E, Dovesi R (1993) Phys State Solids (b) 177:157
28. Dovesi R, FreyriaFava C, Aprà E, Saunders VR, Harrison NM (1992) Phil Trans R Soc Lond A 341:203
29. Becke AD (1993) J Chem Phys 98:5648
30. Lee C, Yang W, Parr RG (1988) Phys Rev B 37:785
31. Corà F, Alfredsson M, Mallia G, Middlemiss DS, Mackrodt WC, Dovesi R, Orlando R (2004) Struct Bond 113:171
32. Dovesi R, Civalleri B, Orlando R, Roetti C, Saunders VR (2005) Rev Comp Chem 21:1
33. Pascale F, Ugliengo P, Civalleri B, Orlando R, D'Arco P, Dovesi R (2002) J Chem Phys 117:5337–5346
34. Pascale F, Ugliengo P, Civalleri B, Orlando R, D'Arco P, Dovesi R (2004) J Chem Phys 121:1005–1013
35. Pascale F, Zicovich-Wilson CM, Orlando R, Roetti C, Ugliengo P, Dovesi R (2005) J Phys Chem B 109:6146
36. Monkhorst HJ, Pack JD (1976) Phys Rev B 8:5188–5192
37. Yuan X, Cormack AN (2002) Comput Mater Sci 24:343–360
38. Malavasi G, Menziani MC, Pedone A, Segre U (2006) J Non-Cryst Solids 352:285
39. Ugliengo P (2005) MOLDRAW: a molecular graphics program to display and manipulate molecular structures. Available at: http://www.moldraw.unito.it
40. Gaskell PH (1995) J Non-Cryst Solids 9:192–193
41. Bar MR, Sauer J (1994) Chem Phys Lett 226:405
42. Hench LL, Splinter RJ, Allen WC, Greenlee TK (1971) J Biomed Mater Res Symp 2:117